Liu, K.; Peng, L.; Zhen, P.; Chen, L.; Song, S.; García Gómez, H.; Sun, C. (2021). ZnCdS Dotted with Highly Dispersed Pt Supported on SiO2 Nanospheres Promoting Photocatalytic Hydrogen Evolution. The Journal of Physical Chemistry C. 125(27):14656-14665. https://doi.org/10.1021/acs.jpcc.1c03535

ZnCdS Dotted with Highly Dispersed Pt Supported on SiO_2 Nanospheres Promoting Photocatalytic Hydrogen Evolution

Ke Liu[a†], Lu Peng[b†], Pingping Zhen[a†], Lichao Chen[a], Shaoqing Song[c], Hermenegildo Garcia[b]*, Chuanzhi Sun[a]*

[a] College of Chemistry, Chemical Engineering and Materials Science, Shandong Provincial Key Laboratory of Clean Production of Fine Chemicals, Institute of Materials and Clean Energy, Shandong Normal University, Jinan 250014, P. R. China, E-mail: suncz@sdnu.edu.cn

[b] Instituto Universitario de Tecnología Química, Consejo Superior de Investigaciones Científicas-Universitat Politécnica de Valencia, Universitat Politecnica de Valencia, Av. De los Naranjos s/n, 46022 Valencia, Spain, E-mail: hgarcia@qim.upv.es

[c] School of Materials Science and Chemical Engineering, Ningbo University, Ningbo 315211, P.R. China

[†] K. Liu, L. Peng and P.P. Zhen contributed equally to this work

Abstract

The efficiency of solar hydrogen evolution closely depends on the fast transfer of charge carriers and the effective use of visible light. In this work, a novel photocatalyst SiO_2/ZnCdS/Pt was successfully prepared to solve these two problems. An artistic structure of the photocatalyst was constructed and the ZnCdS was successfully wrapped on the surface of SiO_2 spheres with uniform Pt nanoparticles (NPs) in the size of 4.1 ± 0.7 nm highly dispersed on the ZnCdS shell through the self-assembly method. Pt NPs can absorb the scattered light in the near field of SiO_2 spheres. With the synergistic effect of SiO_2 spheres and small highly dispersed Pt nanoparticles, the absorption of visible light was significantly promoted. Meanwhile, the electron-hole recombination was also effectively inhibited, thus improving the photocatalytic activity. The hydrogen production activity of the highly efficient photocatalyst was as high as 8.3 mmol g^{-1} h^{-1} under visible light ($\lambda > 420$ nm). The photocatalytic activity of SiO_2/ZnCdS/Pt was 2.9 times higher than that of ZnCdS/Pt photocatalyst.

Keywords: visible light, photocatalytic hydrogen evolution, self-assembly, synergistic effect, SiO_2, Pt NPs

1. Introduction

With the increase of public environmental awareness and the intensification of energy consumption, the development of renewable energy has attracted widespread attention.[1-4] Solar energy is considered as the cleanest, abundant, inextinguishable and most reliable energy source. Therefore, converting solar energy into a form of easy-to-use energy vector has become a hot topic in scientific research. Hydrogen has been proposed as a substitute for fossil energy, and the decomposition of water into hydrogen under illumination is considered to be one of the most promising solar energy utilization methods.[5, 6] There was an upsurge in photocatalysis after Fujishima and Honda reported the water decomposition reaction on TiO_2 for the first time in 1972.[7-12] However, TiO_2 has a wide band gap and low visible light utilization, which limits the photocatalytic activity under natural sunlight illumination.[13] Therefore, current research of photocatalysis has mainly focused on the development of semiconductor materials with narrow band gap and highly efficient visible-light response.

Over the past 50 years, a variety of semiconductors has been developed for hydrogen production, especially metal sulphides.[14-17] As a bimetallic solid solution, ZnCdS has better performance than CdS, ZnS and ZnS/CdS mixture.[18] Compared with ZnS, ZnCdS has a suitable band gap to absorb solar light and an appropriate band alignment for water splitting, which is conducive to the generation of hydrogen. But for CdS, the addition of ZnS not only overcomes the shortcomings of photocorrosion, but diminishes the environmental concern caused by Cd toxicity.[16, 19] However, the occurrence in a large extent of photo-generated electron-hole recombination and low quantum yields limit its application.[20] In order to improve the photocatalytic activity of ZnCdS, various methods have been used, such as the adjustment of morphology, [21-25] the addition of co-catalysts, [26-31] and the construction of heterojunctions.[25, 32-34]

In this work, ZnCdS was wrapped on SiO_2 spheres with a diameter of 700-800 nm, which effectively inhibits the large-scale aggregation of ZnCdS particles. In addition, Pt nanoparticles (NPs) as co-catalysts were supported on the surface of ZnCdS by electrostatic interaction. Compared with the traditional photo-deposition method, smaller Pt NPs with more uniform particle size distribution were deposited by self-assembly. Meanwhile, the synergistic effect of SiO_2 spheres and Pt NPs not only promotes the absorption of visible light, but facilitates charge separation and transfer, thereby significantly enhancing the photocatalytic hydrogen production activity. The hydrogen production activity of SiO_2/ZnCdS/Pt is as high as 8.3 mmol g^{-1} h^{-1}, which is 27 times higher than that of pure ZnCdS and 2.9 times of ZnCdS/Pt. Furthermore, the introduction of SiO_2 spheres further greatly reduced photocorrosion, significantly increasing ZnCdS stability.

2. Experimental

2.1 Synthesis of Samples

1. Synthesis of SiO_2 spheres: SiO_2 spheres were prepared via the Stöber method. In a typical synthesis procedure, 2 mL of tetraethyl orthosilicate (TEOS) was injected into a mixture of 40 mL of isopropanol, 1 mL of deionized H_2O and 2 mL of $NH_3 \cdot H_2O$ (10.5 M) under magnetic stirring. After reacting for 4 h at room temperature, the colloidal spheres were collected by centrifugation at 8000 rpm for 6 min and washed with deionized water twice. Then, the sediment was dried at 60 °C to obtain SiO_2 spheres.

2. Surface modification of SiO_2 spheres: 0.1 g of SiO_2 spheres were dissolved in 30 mL of deionized water followed the ultrasonic for 20 min, then 0.03 g ethylenediaminetetraacetic acid (EDTA) was dissolved in the above solution with the continuous stirring for 24 h at the

temperature of 80 °C. After natural cooling, the products were collected by centrifugation and washed with ethanol and deionized water for three times, and then dried at 60 °C for 12 h in air. The as-prepared samples were marked as SiO_2/EDTA.

3. Synthesis of SiO_2/ZnCdS composites: SiO_2/ZnCdS were synthesized through a facile water bath reaction. Typically, 0.1 g of SiO_2/EDTA were dissolved in 30 mL of deionized water followed the ultrasonic for 20 min, and then an amount of cadmium acetate and zinc acetate were dissolved in the above solution with continuous stirring until the Cd^{2+} and Zn^{2+} were completely dissolved. After that, quantitative thioacetamide (50% excess to stoichiometric amounts of cadmium acetate) was added into the above suspension, the mixture was put into an 80 °C water bath for 6 h with continuous stirring. After the reaction was over and naturally cooled, the products were collected by centrifugation and washed with ethanol and deionized water for three times, and then dried at 60 °C for 12 h in air. Besides, the pure CdZnS was also synthesized with the above method but without the adding of SiO_2/EDTA.

4. Surface modification of SiO_2/ZnCdS: To functionalize the surface of SiO_2/ZnCdS with the positive charge, 0.4 g of the as-obtained SiO_2/ZnCdS was first dispersed in 200 mL of ethanol by sufficient sonication, followed by the addition of 2 mL of 3-aminopropyl-triethoxysilane (APTES). Then, the mixture was kept at 60 °C for 4 h with stirring. Afterwards, APTES-SiO_2/ZnCdS spheres were rinsed with ethanol to remove the remaining APTES moiety and then dried at 60 °C for further use.

5. Preparation of citrate-stabilized Pt nanoparticles (NPs): Citrate-stabilized Pt NPs were synthesized according to the previous report. Typically, 26 mL of sodium citrate aqueous solution (2.8 mM) was added to 50 mL of hexachloroplatinic (IV) acid aqueous solution (0.4 mM) at room temperature. The mixture was stirred to blend well and then 5 mL of $NaBH_4$ (12

mM) was added dropwise with vigorous stirring. The pale-yellow solution turned dark-brown in 5 min and was kept stirring for 4 h. The as-obtained Pt colloids should be stored in a refrigerator at 4 °C for further use.

6. Synthesis of SiO_2/ZnCdS/Pt composites: A certain amount of negatively-charged Pt colloids (0.15 mM) was introduced dropwise into the APTES-modified SiO_2/ZnCdS aqueous suspension (1 mg/mL). The mixture was stirred vigorously for 1 h and then washed with deionized water twice. The sediment was dried at 60 °C and then the supported SiO_2/ZnCdS/Pt composites were obtained.

7. Synthesis of SiO_2/ZnCdS/d-Pt: The SiO_2/ZnCdS/d-Pt composite photocatalysts were synthesized by photodeposition method. In detail, the prepared SiO_2/ZnCdS samples (0.2 g) were dispersed in 200 ml aqueous solution containing 10 vol% triethanolamine (TEOA), a certain amount of H_2PtCl_6 solution in a quartz flask. Then, other residual gases of the mixed system were removed through the vacuum. This suspension was stirred and irradiated for 30 min under UV-vis light (300 W Xe lamp). After that, the product was filtered and washed with distilled water, and finally dried in a vacuum at 60 °C overnight.

2.2 Characterizations

X-ray diffraction (XRD) patterns of the samples were recorded on a Philips X' pert Pro diffractometer with Cu Kα radiation (λ = 0.15418 nm). The Brunauer-Emmett-Teller (BET) specific surface areas were measured using the Micromeritics ASAP-2020 analyzer at 77 K. The high-resolution transmission electron micrographs (HRTEM) of the samples were obtained using a JEM-2100 transmission electron microscope at an acceleration voltage of 200 kV. Inductively coupled plasma-optical emission spectrometry (ICP-OES) was performed on Thermo Scientific

iCAP 7000 apparatus to determine the actual concentration of the elements in the samples. The Escalab 250 Xi (Thermo Scientific) X-ray photoelectron spectrometer with an Al-Kα X-ray (hν = 1486.6 eV) was used to perform the X-ray photoelectron spectroscopy (XPS) analysis. The binding energy values obtained in the XPS analysis were corrected by the C 1s peak of 284.6 eV. UV-vis absorption spectra were measured by a UV-visible spectrometer (X-3, YuanXi Instruments). Photoluminescence (PL) spectra were recorded using the FLS-980 Edinburgh Fluorescence Spectrophotometer. Transient photocurrent response, electrochemical impedance spectroscopy (EIS) spectra were measured on a CHI-660C electrochemical workstation with a standard three-electrode system. The three-electrode configuration includes a working electrode, a platinum plate as a counter electrode, and Ag/AgCl (saturated KCl) as a reference electrode. The light source was the 300 W xenon lamp with a 420 nm cut-off filter and the electrolyte solution was the 0.1 M Na_2SO_4 solution. Transient photocurrent response and EIS were measured at 0.5 V (vs.Ag/AgCl). The working electrodes were prepared by dispersing 2 mg sample to 2 mL ethanol. Then, 10 μL of 0.25% Nafion was added, followed by sonication for 30 min to obtain a slurry. The suspension was dropped onto a conductive glass (FTO) sheet (1 cm × 2 cm) and dried in an oven at 100 °C for 10 h. Electron paramagnetic resonance (EPR) signals were recorded on a Bruker A300-10/12/S-LC spectrometer. The 2-methyl-N-(4-pyridinylmethylene)-2-propanamine N, N'-dioxide (POBN) was used as a trapping agent.

2.3 Photocatalytic Hydrogen Evolution Test

The photocatalytic hydrogen production system was performed in a quartz flask. Specific steps: 5mg of the photocatalyst was dispersed by magnetic stirring into an aqueous solution composed of 10 mL water with 0.35 M Na_2S/0.25 M Na_2SO_3. This system was evacuated to remove the residual gas. Then, the photocatalytic system was irradiated with a 300 W Xe arc

lamp with an ultraviolet cutoff filter (λ > 420 nm) under magnetic stirring. The hydrogen production is analyzed by a gas chromatograph (GC-7900, TCD, Ar as the carrier gas, and 5 Å molecular sieve column.)

The external quantum efficiency (EQE) was measured at 405 nm, 420 nm, 450 nm and 500 nm monochromatic wavelength which were obtained by the 300 W Xe lamp with a monochromator. The output intensities were determined by a NOVA II laser power meter (Ophir Photonics). The distance between the light source and the catalytic reaction device is 5 cm. The EQE was calculated through the following Eq(1). The EQE experiment was performed in a sealed 20 ml quartz bottle. 5 mg photocatalyst was dispersed by magnetic stirring into the 10 ml aqueous solution containing 0.35 M Na_2S/0.25 M Na_2SO_3. Then, the system was evacuated and argon was bubbled for 10 min. The light source of the photocatalytic system was a 300 W xenon lamp with different filters (λ = 405 nm, 420 nm, 450 nm, 500 nm and 650 nm).

$$EQE\ (\%) = \frac{number\ of\ reacted\ eletrons}{number\ of\ incident\ photons} \times 100\ \%$$

$$= \frac{number\ of\ evolved\ H_2\ \ molecules \times 2}{number\ of\ incident\ photons} \times 100\ \%$$

3. Results and Discussion

Scheme 1 illustrates the synthesis of the SiO_2/ZnCdS/Pt. Spherical SiO_2 was prepared following the traditional Stöber method.[35] Then, SiO_2 spheres were modified by ethylenediaminetetraacetic acid (EDTA) to generate highly negative charges on the surface. As shown in **Figure S1**, the zeta potential of SiO_2 spheres changed from -8.09 mV to -46.3 mV after the modification of EDTA. Therefore, the subsequently added positively charged Cd^{2+} and Zn^{2+} were strongly adsorbed on the surface of SiO_2 spheres by electrostatic attraction, while S^{2-} released from thioacetamide slowly combines with metal ions, forming ZnCdS wrapped on the

surface of SiO_2 spheres. Then, the obtained SiO_2/ZnCdS was modified with (3-aminopropyl) tiethoxysilane (APTES) to make the surface positively charged, as shown in **Figure S1**. Afterwards, the negatively charged platinum colloid with a zeta potential of -25 mV was added to obtain the final catalyst SiO_2/ZnCdS/Pt.

[Scheme 1 near here]

3.1 Photocatalytic activity for H_2 evolution

Figure 1 shows the hydrogen production activity of different catalysts under visible light irradiation ($\lambda > 420$ nm). As shown in **Figure 1(a)**, hydrogen production activity of samples with different mass ratios of SiO_2 and ZnCdS were studied, in which the sample with SiO_2 and ZnCdS mass ratio of 1 showd the highest hydrogen production activity reaching up to 1 mmol g^{-1} h^{-1}. **Figure 1(b)** shows the influence of Pt loading in SiO_2/ZnCdS/Pt on H_2 evolution. When the Pt loading in SiO_2/ZnCdS/Pt is 2.5 wt.%, the hydrogen production activity is as high as 8.3 mmol g^{-1} h^{-1}, which is 4.2 times higher than that of 0.6 wt.% Pt, 2.5 times of 1.9 wt. % Pt and 2.8 times of 3.1 wt.% Pt. As shown in **Figure 1(c)**, the hydrogen production activity of pure ZnCdS is about 0.3 mmol g^{-1} h^{-1}, while the activity is increased to 1 mmol g^{-1} h^{-1} after adhering ZnCdS on SiO_2 spheres. In addition, the hydrogen production activity of ZnCdS/Pt is improved to 2.9 mmol g^{-1} h^{-1} by Pt NPs addition. It appears that the introduction of SiO_2 or Pt NPs is beneficial for the improvement of the photocatalytic activity. Therefore, when Pt NPs are loaded on the surface of SiO_2/ZnCdS, the hydrogen production activity of SiO_2/ZnCdS/Pt is 27 times higher than that of pure ZnCdS, 8 times of SiO_2/ZnCdS and 2.9 times of ZnCdS/Pt, indicating that structuration of the components on the SiO_2 spheres causes a synergistic effect between SiO_2 and Pt NPs, which enhances the photocatalytic performance of the system. Meanwhile, catalyst SiO_2/ZnCdS/d-Pt prepared by traditional photo-depositing Pt on SiO_2/ZnCdS was used for comparison. As can be

seen in **Figure 1(c)** and **Table S1**, when the Pt content in the two catalysts is similar, the hydrogen production activity of SiO_2/ZnCdS/d-Pt is only 3.5 mmol g^{-1} h^{-1}, less than half of SiO_2/ZnCdS/Pt. Some other ZnCdS-based catalysts using precious metals as promoters are shown **Table S2**, and their hydrogen production activities are much lower than that of our novel catalysts.

As shown in **Figure 1(d)**, after four cycles, the hydrogen production activity of SiO_2/ZnCdS/Pt only decreases slightly, remaining essentially constant, indicating good stability. The external quantum efficiency (EQE) of SiO_2/ZnCdS/Pt upon monochromatic light irradiation is shown in **Table S3**, and the EQE at 420 nm reaches a high value of 8.7 %.

[Figure 1 near here]

3.2 Structure Characterization

X-ray diffraction (XRD) was used to investigate the phase structure of the samples. **Figure S2** shows XRD patterns of the prepared five samples. There are three different distinctive diffraction peaks of ZnCdS located at 2θ = 26.7°, 44.2° and 52.2°, corresponding to (002), (110) and (112) planes of ZnCdS, respectively.[36] In the case of SiO_2/ZnCdS and SiO_2/ZnCdS/Pt samples, all peaks mentioned above can be observed, but they become wider due to the lower crystallinity of ZnCdS and the close position of diffraction angles of SiO_2 (2θ = 23°) and ZnCdS (2θ = 26.7°).[37] In addition, there are no obvious peaks attributable to Pt species. A fact that can be understood that the low Pt loading and high dispersion of Pt NPs with small particle size in samples SiO_2/ZnCdS/Pt as well as ZnCdS/Pt.

Specific surface area and pore size distribution of the samples were obtained through the N_2 adsorption and desorption isotherms. **Figure S3** shows the isotherms of these samples. These

measurements clearly show that all tested samples can be categorized as type IV isotherms with H3 hysteresis loops, which suggests that there is micro-mesoporous structure in the catalysts.[38, 39] The specific surface area of ZnCdS, ZnCdS/Pt, SiO_2/ZnCdS and SiO_2/ZnCdS/Pt are shown in **Table S4**. Among the four samples, SiO_2/ZnCdS/Pt has the smallest specific surface area, but its photocatalytic hydrogen production activity is the highest, indicating that the specific surface area of this series of catalysts is not the main decisive factor affecting its catalytic activity.

The microstructure and morphology of samples were investigated. As shown in **Figure 2(a)**, the pure SiO_2 shows a spherical shape with a diameter of about 700-800 nm and a smooth surface. **Figure 2(b)** displays the TEM image of pure ZnCdS, which easily undergo agglomeration. Interplanar distance of 3.2 Å corresponding to the (002) plane of ZnCdS was measured in **Figure S4**, proving the successful synthesis of ZnCdS. The TEM images clearly reveal the structure of SiO_2/ZnCdS, SiO_2/ZnCdS/Pt and SiO_2/ZnCdS/d-Pt samples. As shown in **Figure 2(c)**, dark spheres were surrounded by a heavier black substance, in which ZnCdS was wrapping SiO_2 spheres, generating a core-shell structure. The image of SiO_2/ZnCdS/Pt was presented in **Figure 2(d)**, the presence of Pt NPs can be observed. Meanwhile, interplanar distance of 2.2 Å corresponding to the (111) plane of Pt was found in **Figure 2(e)**, proving the existence of Pt NPs. In addition, measurement of the interplanar distance of 3.2 Å corresponding to the (002) plane of ZnCdS was presented in **Figure 2(e)**, further indicating that ZnCdS was located at the outer layer of SiO_2 spheres.[40, 41] Deposition of ZnCdS on SiO_2 spheres inhibits its aggregation, which may result in a shorter charge transfer path between the layered ZnCdS and Pt NPs and significantly accelerate the charge transfer. HRTEM image of SiO_2/ZnCdS/d-Pt prepared by photo-deposition presented in **Figure 2(f)** shows that the Pt NPs are dispersed on the outer layer of SiO_2/ZnCdS surface. Furthermore, the dark-field transmission electron microscopy

(DF-TEM) images of SiO_2/ZnCdS/Pt and SiO_2/ZnCdS/d-Pt, given in **Figures 2(g)** and **2(h)**, clearly shows that the Pt NPs of SiO_2/ZnCdS/Pt are much smaller than those of SiO_2/ZnCdS/d-Pt. The statistical determination of the Pt NP size provided in **Figure S5** indicates that the average Pt NP size of SiO_2/ZnCdS/Pt is 4.1 ± 0.7 nm, while Pt NPs on SiO_2/ZnCdS/d-Pt have a much larger average particle size of 15.4 ± 2.3 nm. Comparing the photocatalytic H_2 production rates of SiO_2/ZnCdS/Pt and SiO_2/ZnCdS/d-Pt, the results establish that smaller, highly-dispersed Pt NPs may give much more exposed active sites and effectively improve the photocatalytic activity, which suggests the size-dependent effect of the Pt NPs on the photocatalytic performance. Energy dispersive spectrum (EDS) elemental mappings of SiO_2/ZnCdS/Pt and SiO_2/ZnCdS/d-Pt are shown in **Figure 2(i-o)** and **Figure S6(a-g)**. The Zn, Cd, S and Pt elements can be detected in SiO_2/ZnCdS/Pt and SiO_2/ZnCdS/d-Pt, and the distribution of the different elements exhibit a spherical shape, which proves that the SiO_2 spheres are coated by ZnCdS, and Pt NPs are highly dispersed on the catalyst surface. In addition, the TEM, HRTEM images and EDS elemental mappings of SiO_2/ZnCdS/Pt after the hydrogen production reaction are shown in **Figure S7**. It is found that the morphology and crystal phase have no observed change after hydrogen production reaction, which proves the stability of the catalyst.

[Figure 2 near here]

X-ray photoelectron spectroscopy (XPS) was used to study the chemical composition and state of photocatalysts. The XPS spectra of SiO_2/ZnCdS/Pt are given in **Figure 3**. As shown in **Figure 3(a)**, there are two peaks located at binding energies of 411.6 eV and 404.9 eV, corresponding to Cd $3d_{3/2}$ and Cd $3d_{5/2}$, respectively, indicating that in SiO_2/ZnCdS/Pt, Cd exists in the form of Cd^{2+}.[42] In **Figure 3(b)**, the XPS spectrum of Zn 2p with two peaks at binding energies of 1044.8 eV and 1021.6 eV, are ascribed to the Zn $2p_{1/2}$ and Zn $2p_{3/2}$, respectively,

indicating that in SiO_2/ZnCdS/Pt, Zn exists in the form of Zn^{2+}.[43] Meanwhile, the S 2p spectrum shown in **Figure 3(c)** with two components at binding energies at 162.6 eV and 161.4 eV can be assigned to S $2p_{1/2}$ and S $2p_{3/2}$, respectively, suggesting the sulfur element in the compound exists in the form of S^{2-}.[18] The Pt 4f spectrum shown in **Figure 3(d)** can be divided into six peaks. Two distinct peaks at 71.1 eV and 74.5 eV are assigned to metallic Pt, and the peaks at 72.0 eV and 75.3 eV are attributed to the Pt^{2+}, the other two peaks at 73.4 and 76.4 are attributed to the PtO_2. Comparing the binding energy of metallic Pt in ZnCdS/Pt and SiO_2/ZnCdS/Pt samples, it appears that peak assigned to metallic Pt locating at the binding energy of 71.3 shifts to 71.1 when ZnCdS/Pt is supported on SiO_2 spheres, indicating that the electron density on Pt NPs increases under this condition, which should favour the electron transfer from ZnCdS to Pt NPs.[44] The atomic ratios of SiO_2/ZnCdS/Pt are shown in **Table S5**, and the ratio of Zn+Cd/S is 1.25. The XPS spectra of SiO_2/ZnCdS/d-Pt are shown in **Figure S8**, suggesting that Cd, Zn, and S exist respectively in the form of Cd^{2+}, Zn^{2+} and S^{2-} in SiO_2/ZnCdS/d-Pt, which are the same as that in SiO_2/ZnCdS/Pt. However, the binding energies of peaks assigned to metallic Pt of SiO_2/ZnCdS/d-Pt sample are higher than that of SiO_2/ZnCdS/Pt sample, suggesting that the electron density of Pt in SiO_2/ZnCdS/Pt is higher than that in SiO_2/ZnCdS/d-Pt, and Pt NPs deposited by self-assemble method facilitate charge accumulation.

[Figure 3 near here]

3.3 Optical and electrochemical properties of photocatalysts

Ultraviolet-visible (UV-vis) spectroscopy was used to study the optical properties of SiO_2, ZnCdS, ZnCdS/Pt, SiO_2/ZnCdS and SiO_2/ZnCdS/Pt. As shown in **Figure 4(a)**, UV-vis spectra demonstrate that all the catalysts have photoabsorption in the visible region except SiO_2. **Figure S9** shows that SiO_2 does not absorb any light and the absorption of Pt NPs appears as a broad

continuous absorption, which is due to the excitation of free electrons from the conduction band to a higher Fermi level.[45] Compared with ZnCdS, the absorption edge of SiO_2/ZnCdS shows no shift, while that of ZnCdS/Pt and SiO_2/ZnCdS/Pt have a significant redshift, which should be caused by the light absorption of Pt NPs. However, the redshift of SiO_2/ZnCdS/Pt is larger than that of ZnCdS/Pt, which is due to the scattered light absorption of Pt NPs in the near-field of SiO_2 spheres.[46, 47]

Photoluminescence spectroscopy (PL) was used for better understanding the relative charge separation efficiency of the photocatalysts. As shown in **Figure 4(b)**, the emission spectra of these catalysts are the same, but their intensities are significantly different. The peak intensity of these samples follows the order of ZnCdS > SiO_2/ZnCdS > ZnCdS/Pt > SiO_2/ZnCdS/Pt. The lower PL intensity indicates the higher efficiency of electron-hole pair recombination.[48, 49] It can be concluded that, after adding highly dispersed Pt NPs, the photogenerated electrons can easily transfer to the surface of the Pt NPs, meanwhile the holes remain in ZnCdS. This charge separation inhibits electron-hole recombination. Time-resolved fluorescence spectra (TRF), as shown in **Figure 4(c)**, illustrates the photogenerated electron transfer of the photocatalysts. In the TRF spectra, decay plots of all catalysts are fitted using the triexponential function. The three lifetimes and corresponding percentage of charge carriers are listed in **Table 1**, in which τ_1, τ_2, and τ_v represent the radiation lifetime, the lifetime of the non-radiation phase and the average lifetime, respectively. Regard the value of τ_1, τ_2, and τ_v, they are the longest for SiO_2/ZnCdS/Pt, while these values are the shortest for ZnCdS, and SiO_2/ZnCdS and ZnCdS/Pt exhibit intermediate values. The longest emission lifetime of SiO_2/ZnCdS/Pt indicates the highest probability of charge carriers participating in the photocatalytic reaction process. Besides charge transfer, energy transfer processes quantitatively measured by the energy transfer rate constant

(K_{ENT}) and energy transfer efficiency (Φ_{ENT}). Compared with other three catalysts, the K_{ENT} and Φ_{ENT} values of SiO_2/ZnCdS/Pt are the highest, suggesting that the structural arrangement of ZnCdS/Pt on the SiO_2 surface is favorable to promote the energy transfer.[50, 51] The results of PL and TRF show that SiO_2 and Pt NPs can inhibit the electron-hole recombination and promote charge transfer, thereby enhancing the photocatalytic performance of the catalyst.

The separation of photogenerated charges and the transfer of electrons can be further investigated by photoelectrochemical experiments. The transient photocurrent response of a photocatalyst may be directly related to the efficiency of photogenerated charge separation.[52] Comparing the photocurrent response of the four catalysts, as shown in **Figure 4(d)**, it appears that the use of SiO_2 spheres as supports and the addition of Pt NPs can accelerate the separation of electron-hole pairs. EIS was measured to determine the contribution of the independent components to the electrochemical properties of different catalysts. The arc radius of the semicircular part of the Nyquist plot reflects the magnitude of the electrode resistance and the surface reaction rate. The smaller the radius of the arc, the easier the charge transfer efficiency from the catalyst to the electrolyte solution is. As shown in **Figure 4(e),** the pure ZnCdS catalyst shows the largest radius and SiO_2/ZnCdS/Pt shows the smallest, indicating that deposition on SiO_2 and the presence of Pt NPs can accelerate charge transfer processes on the catalyst.[53] The overpotentials and currents of catalysts were obtained through the polarization curves in **Figure 4(f)**. SiO_2/ZnCdS/Pt exhibits the highest current density and the lowest overpotential, indicating that the structuration on SiO_2 and adsorption of Pt favors the process of reducing protons to hydrogen.[45]

[Figure 4 near here]

[Table 1 near here]

3.4 Photocatalytic mechanism of H_2 production

Electron paramagnetic resonance (EPR) spectroscopy can detect free radicals generated during the reaction, which can be involved as reaction intermediates in the mechanism of the photocatalytic reaction. **Figure 5** shows the electron paramagnetic resonance spectra upon performing the photocatalytic H_2 generation under visible light by four photocatalysts in the presence of 2-methyl-N-(4-pyridinylmethylene)-2-propanamine N,N'-dioxide (POBN) as spin trapping agent. Under these conditions, the peaks of POBN-H• adducts were recorded for all catalysts, confirming that H• radicals are intermediate species in the process of photocatalytic hydrogen production.[54, 55] The peak intensities of POBN-H• for the four catalysts follow the order of ZnCdS < SiO_2/ZnCdS < ZnCdS/Pt < SiO_2/ZnCdS/Pt, consistent with their hydrogen production activity, indicating that the formation of H• radicals is enhanced by the synergistic effect of SiO_2 and Pt NPs, thereby improving the photocatalytic hydrogen production activity.

[Figure 5 near here]

Based on the above discussion, there are three main reasons for the improvement of SiO_2/ZnCdS/Pt photocatalytic activity, as shown in **Scheme 2**: 1) Pt NPs can absorb the scattered light in the near field of SiO_2 spheres, which promotes the absorption and utilization of visible light, generating hot electrons on the catalyst; 2) The core-shell structure of ZnCdS@SiO_2 inhibits the aggregation of ZnCdS and shortens the charge transfer path between the ZnCdS nanoplatelets and Pt NPs, which significantly accelerates the charge transfer and effectively inhibits electron-hole recombination; 3) Photogenerated electrons on ZnCdS can easily transfer to the surface of the Pt NPs, which promotes the electron-hole separation and accelerates the photocatalytic hydrogen reaction.

[Scheme 2 near here]

4. Conclusions

A highly efficient SiO_2/ZnCdS/Pt was successfully prepared through the self-assembly method of which hydrogen production activity under visible light was as high as 8.3 mmol g^{-1} h^{-1}. For this SiO_2/ZnCdS/Pt photocatalyst, the ZnCdS was successfully supported on the surface of SiO_2 spheres by sulfidation of adsorbed Zn^{2+} and Cd^{2+} cations, and Pt NPs with the uniform particle size distribution of 4.1 ± 0.7 nm were electrostatically attached to the SiO_2/ZnCdS composite. The Pt NPs on SiO_2/ZnCdS/Pt photocatalyst are much smaller and more efficient than those prepared by the photo-deposition method. The synergistic effect of SiO_2 spheres and Pt NPs not only promotes the absorption of visible light, but accelerates the separation and transfer of charges, therefore, significantly increasing the rate of hydrogen production. The photocatalytic activity of SiO_2/ZnCdS/Pt is 2.9 times higher than that of ZnCdS/Pt and 2.4 times of SiO_2/ZnCdS/d-Pt, respectively. These results illustrate the benefits of structuration for multifunctional photocatalyst and the importance of design and appropriate synthesis methods to optimize the visible light photocatalytic hydrogen production.

Supporting Information

The ICP analysis of samples with different Pt loadings; Comparison of photocatalytic hydrogen evolution performance of water splitting over previously reported ZnCdS-based photocatalysts; EQE values calculated at different wavelength; The specific surface area of different samples; Atomic ratios of the elements determined from the XPS spectra; Zeta potential of SiO_2, SiO_2/EDTA, SiO_2/ZnCdS, SiO_2/ZnCdS/APTES and Pt NPs; XRD patterns of SiO_2, ZnCdS, ZnCdS/Pt, SiO_2/ZnCdS and SiO_2/ZnCdS/Pt; Nitrogen adsorption-desorption isotherms of

ZnCdS, ZnCdS/Pt, SiO_2/ZnCdS and SiO_2/ZnCdS/Pt samples; HRTEM image of ZnCdS; DF-TEM image of SiO_2/ZnCdS/Pt and the corresponding Pt NPs size distribution histogram, DF-TEM image of SiO_2/ZnCdS/d-Pt and the corresponding Pt NPs size distribution histogram; DF-TEM image and Energy dispersive spectrometer (EDS) elemental mappings of SiO_2/ZnCdS/d-Pt; TEM image, HRTEM image, DF-TEM image and EDS elemental mappings of SiO_2/ZnCdS/Pt after hydrogen production reaction; High-resolution XPS spectra of Cd 3d, Zn 2p, S 2p of SiO_2/ZnCdS/d-Pt and Pt 4f of SiO_2/ZnCdS/Pt and SiO_2/ZnCdS/d-Pt; and UV-vis diffuse reflectance spectra of SiO_2 and Pt nanoparticles.

Acknowledgements

This work was supported by the National Natural Science Foundation of China (21976111), Shandong Provincial Natural Science Foundation (ZR2019MB052), and Large Instrument Open Foundation of Shandong Normal University (KFJJ2019004; KFJJ2021006).

References

(1) Lewis, N. S.; Nocera, D. G. Powering the planet: chemical challenges in solar energy utilization. *Proc. Natl. Acad. Sci. U.S.A.* **2006,** *103* (43), 15729-35.
(2) Lubitz, W.; Reijerse, E. J.; Messinger, J. Solar water-splitting into H_2 and O_2: design principles of photosystem II and hydrogenases. *Energy Environ. Sci.* **2008,** *1* (1), 15.
(3) Hambourger, M.; Moore, G. F.; Kramer, D. M.; Gust, D.; Moore, A. L.; Moore, T. A. Biology and technology for photochemical fuel production. *Chem. Soc. Rev.* **2009,** *38* (1), 25-35.
(4) Zhang, S.; Li, J.; Zeng, M.; Li, J.; Xu, J.; Wang, X. Bandgap engineering and mechanism study of nonmetal and metal ion codoped carbon nitride: C+Fe as an example. *Chemistry* **2014,** *20* (31), 9805-12.
(5) Kudo, A. Recent progress in the development of visible light-driven powdered photocatalysts for water splitting. Int. J. Hydrogen Energy **2007,** *32* (14), 2673-2678.
(6) Jiang, N.; Tang, Q.; Sheng, M.; You, B.; Jiang, D.-e.; Sun, Y. Nickel sulfides for electrocatalytic hydrogen evolution under alkaline conditions: a case study of crystalline NiS, NiS_2, and Ni_3S_2 nanoparticles. Catal. Sci. Technol. **2016,** *6* (4), 1077-1084.
(7) Zheng, M.; Ding, Y.; Yu, L.; Du, X.; Zhao, Y. In Situ Grown Pristine Cobalt Sulfide as Bifunctional Photocatalyst for Hydrogen and Oxygen Evolution. *Adv. Funct. Mater.* **2017,** *27* (11), 1605846.
(8) Sun, Y.; Liu, C.; Grauer, D. C.; Yano, J.; Long, J. R.; Yang, P.; Chang, C. J. Electrodeposited cobalt-sulfide catalyst for electrochemical and photoelectrochemical hydrogen generation from water. *J. Am. Chem. Soc.* **2013,** *135* (47), 17699-702.
(9) Liao, L.; Zhang, Q.; Su, Z.; Zhao, Z.; Wang, Y.; Li, Y.; Lu, X.; Wei, D.; Feng, G.; Yu, Q.; etc. Efficient solar water-splitting using a nanocrystalline CoO photocatalyst. *Nat Nanotechnol* **2014,** *9* (1), 69-73.
(10) Rockafellow, E. M.; Stewart, L. K.; Jenks, W. S. Is sulfur-doped TiO_2 an effective visible light photocatalyst for remediation? *Appl. Catal. B: Environ.* **2009,** *91* (1-2), 554-562.
(11) Han, C.; Pelaez, M.; Likodimos, V.; Kontos, A. G.; Falaras, P.; O'Shea, K.; Dionysiou, D. D. Innovative visible light-activated sulfur doped TiO_2 films for water treatment. *Appl. Catal. B: Environ.* **2011,** *107* (1-2), 77-87.
(12) Fujishima, A.; Honda, K. Electrochemical photolysis of water at a semiconductor electrode. *Nature* **1972,** *238* (5358), 37-8.
(13) Wang, M.; Jin, C.; Li, Z.; You, M.; Zhang, Y.; Zhu, T. The effects of bismuth (III) doping and ultrathin nanosheets construction on the photocatalytic performance of graphitic carbon nitride for antibiotic degradation. *J. Colloid Interface Sci.* **2019,** *533*, 513-525.
(14) Wang, Z.; Qi, Z.; Fan, X.; Leung, D. Y. C.; Long, J.; Zhang, Z.; Miao, T.; Meng, S.; Chen, S.; Fu, X. Intimately Contacted Ni_2P on CdS Nanorods for Highly Efficient Photocatalytic H_2 Evolution: New Phosphidation Route and the Interfacial Separation Mechanism of Charge Carriers. *Appl. Catal. B: Environ.* **2021,** *281*, 119443.
(15) Zhao, H.; Dong, Y.; Jiang, P.; Wang, G.; Miao, H.; Wu, R.; Kong, L.; Zhang, J.; Zhang, C. Light-Assisted Preparation of a ZnO/CdS Nanocomposite for Enhanced Photocatalytic H_2 Evolution: An Insight into Importance of in Situ Generated ZnS. *ACS Sustain. Chem. Eng.* **2015,** *3* (5), 969-977.
(16) Li, Q.; Meng, H.; Zhou, P.; Zheng, Y.; Wang, J.; Yu, J.; Gong, J. $Zn_{1-x}Cd_xS$ Solid Solutions with Controlled Bandgap and Enhanced Visible-Light Photocatalytic H_2-Production Activity. *ACS Catal.* **2013,** *3* (5), 882-889.

(17) Tosun, B. S.; Pettit, C.; Campbell, S. A.; Aydil, E. S. Structure and composition of $Zn_xCd_{1-x}S$ films synthesized through chemical bath deposition. *ACS Appl. Mater. Interfaces* **2012,** *4* (7), 3676-84.
(18) Jin, Z.; Liu, Y.; Hao, X. Self-assembly of zinc cadmium sulfide nanorods into nanoflowers with enhanced photocatalytic hydrogen production activity. *J. Colloid Interface Sci.* **2020,** *567*, 357-368.
(19) Song, L.; liu, D.; Zhang, S.; Wei, J. WO_3 cocatalyst improves hydrogen evolution capacity of ZnCdS under visible light irradiation. *Int. J. Hydrogen Energ.* **2019,** *44* (31), 16327-16335.
(20) Shen, R.; Ding, Y.; Li, S.; Zhang, P.; Xiang, Q.; Ng, Y. H.; Li, X. Constructing low-cost Ni_3C/twin-crystal $Zn_{0.5}Cd_{0.5}S$ heterojunction/homojunction nanohybrids for efficient photocatalytic H_2 evolution. *Chin. J. Catal.* **2021,** *42* (1), 25-36.
(21) Chen, J.; Chen, J.; Li, Y. Hollow ZnCdS dodecahedral cages for highly efficient visible-light-driven hydrogen generation. *J. Mate. Chem. A* **2017,** *5* (46), 24116-24125.
(22) Chen, J.; Lv, S.; Shen, Z.; Tian, P.; Chen, J.; Li, Y. Novel ZnCdS Quantum Dots Engineering for Enhanced Visible-Light-Driven Hydrogen Evolution. *ACS Sustain. Chem. Eng.* **2019,** *7* (16), 13805-13814.
(23) Zhou, X.; Zhang, N.; Yin, L.; Zhao, Y.; Zhang, B. Few-layered WS_2 nanosheets onto 1D CdS@ZnCdS as efficient visible-light photocatalyst for hydrogen evolution. *Ceram. Int.* **2020,** *46* (16), 26100-26108.
(24) Liu, T.; Li, Q.; Qiu, S.; Wang, Q.; Peng, X.; Yuan, H.; Wang, X. Construction of $Zn_{0.5}Cd_{0.5}S$ nanosheets and the hybridization with onion-like carbon for enhanced photocatalytic hydrogen production. *Appl. Surf. Sci.* **2020,** *525*, 146586.
(25) Jiang, Z.; Chen, Q.; Zheng, Q.; Shen, R.; Zhang, P.; Li, X. Constructing 1D/2D Schottky-Based Heterojunctions between $Mn_{0.2}Cd_{0.8}S$ Nanorods and Ti_3C_2 Nanosheets for Boosted Photocatalytic H_2 Evolution. *Acta. Phys-Chim Sin* **2020,** *0* (0), 2010059-0.
(26) Shu, D.; Wang, H.; Wang, Y.; Li, Y.; Liu, X.; Chen, X.; Peng, X.; Wang, X.; Ruterana, P.; Wang, H. Composition dependent activity of $Fe_{1-x}Pt_x$ decorated ZnCdS nanocrystals for photocatalytic hydrogen evolution. *Int. J. Hydrogen Energy* **2016,** *42* (32), 20888-20894.
(27) Liu, H.; Su, P.; Jin, Z.; Ma, Q. Enhanced Hydrogen Evolution over Sea-Urchin-Structure NiCoP Decorated ZnCdS Photocatalyst. Catal. Lett. **2020,** *150* (10), 2937-2950.
(28) Song, L.; Zhang, S.; Liu, D.; Sun, S.; Wei, J. High-performance hydrogen evolution of NiB/ZnCdS under visible light irradiation. Int. J. Hydrogen Energy. **2020,** *45* (15), 8234-8242.
(29) Wang, F.; Su, Y.; Min, S.; Li, Y.; Lei, Y.; Hou, J. Synergistically enhanced photocatalytic hydrogen evolution performance of ZnCdS by co-loading graphene quantum dots and PdS dual cocatalysts under visible light. J. Solid State Chem. **2018,** *260*, 23-30.
(30) Ren, D.; Liang, Z.; Ng, Y. H.; Zhang, P.; Xiang, Q.; Li, X. Strongly coupled 2D-2D nanojunctions between P-doped Ni_2S (Ni_2SP) cocatalysts and CdS nanosheets for efficient photocatalytic H_2 evolution. *Chem. Eng. J.* **2020,** *390*, 124496.
(31) Liang, Z.; Shen, R.; Ng, Y. H.; Zhang, P.; Xiang, Q.; Li, X. A review on 2D MoS_2 cocatalysts in photocatalytic H_2 production. *J. Mater. Sci. Technol.* **2020,** *56*, 89-121.
(32) Zhang, X.; Peng, J.; Ding, Y.; Zheng, D.; Lin, Y.; Chen, Y.; Gao, W. Rationally designed hierarchical hollow ZnCdS@MoS_2 heterostructured cages with efficient separation of photogenerated carriers for photoelectrochemical aptasensing of lincomycin. *Sens. Actuators, B* **2020,** *306*, 127552.

(33) Imran, M.; Yousaf, A. B.; Kasak, P.; Zeb, A.; Zaidi, S. J. Highly efficient sustainable photocatalytic Z-scheme hydrogen production from an α-Fe_2O_3 engineered ZnCdS heterostructure. *Chin. J. Catal.* **2017,** *353*, 81-88.
(34) Shen, R.; Ren, D.; Ding, Y.; Guan, Y.; Ng, Y. H.; Zhang, P.; Li, X. Nanostructured CdS for efficient photocatalytic H_2 evolution: A review. Sci. China Mater. **2020,** *63* (11), 2153-2188.
(35) Vacassy, R.; Flatt, R. J.; Hofmann, H.; Choi, K. S.; Singh, R. K. Synthesis of Microporous Silica Spheres. *J. Colloid Interface Sci.* **2000,** *227* (2), 302-315.
(36) Lin, S.; Zhang, Y.; You, Y.; Zeng, C.; Xiao, X.; Ma, T.; Huang, H. Bifunctional Hydrogen Production and Storage on 0D-1D Heterojunction of $Cd_{0.5}$ $Zn_{0.5}S$@Halloysites. *Adv. Funct. Mater.* **2019,** *29* (39), 1903825.
(37) Oh, W. C.; Nguyen, D. C. T.; Areerob, Y. Novel cadmium oxide-graphene nanocomposite grown on mesoporous silica for simultaneous photocatalytic H_2-evolution. *Chemosphere* **2020,** *239*, 124825.
(38) Sun, C.; Zhang, H.; Liu, H.; Zheng, X.; Zou, W.; Dong, L.; Qi, L. Enhanced activity of visible-light photocatalytic H_2 evolution of sulfur-doped g-C_3N_4 photocatalyst via nanoparticle metal Ni as cocatalyst. *Appl. Catal. B: Environ.* **2018,** *235*, 66-74.
(39) Zheng, Y.; Yu, Z.; Lin, F.; Guo, F.; Alamry, K. A.; Taib, L. A.; Asiri, A. M.; Wang, X. Sulfur-Doped Carbon Nitride Polymers for Photocatalytic Degradation of Organic Pollutant and Reduction of Cr(VI). *Molecules* **2017,** *22* (4).
(40) Chen, J.; Shen, Z.; Lv, S.; Shen, K.; Wu, R.; Jiang, X.-f.; Fan, T.; Chen, J.; Li, Y. Fabricating sandwich-shelled ZnCdS/ZnO/ZnCdS dodecahedral cages with "one stone" as Z-scheme photocatalysts for highly efficient hydrogen production. *J. Mate. Chem. A* **2018,** *6* (40), 19631-19642.
(41) Yang, T.; Zhang, C.; Li, H.; Wang, Z.; Zhang, J.; Wang, X.; Chai, Z. Pt/N-rGO/Nb_4N_5 Electrocatalyst with Multilayered Structure and Ternary Synergy for Promoting Alcohol Oxidation. *J. Alloys Compd.* **2020,** *845*, 156117.
(42) Biswal, N.; Das, D. P.; Martha, S.; Parida, K. M. Efficient hydrogen production by composite photocatalyst CdS-ZnS/Zirconium-titanium phosphate (ZTP) under visible light illumination. *Int. J. Hydrogen Energy* **2011,** *36* (21), 13452-13460.
(43) Dai, D.; Wang, L.; Xiao, N.; Li, S.; Xu, H.; Liu, S.; Xu, B.; Lv, D.; Gao, Y.; Song, W.; etc. In-situ synthesis of Ni_2P co-catalyst decorated $Zn_{0.5}Cd_{0.5}S$ nanorods for high-quantum-yield photocatalytic hydrogen production under visible light irradiation. *Appl. Catal. B: Environ.* **2018,** *233*, 194-201.
(44) Zhang, N.; Qi, M. Y.; Yuan, L.; Fu, X.; Tang, Z. R.; Gong, J.; Xu, Y. J. Broadband Light Harvesting and Unidirectional Electron Flow for Efficient Electron Accumulation for Hydrogen Generation. *Angew. Chem. Int. Ed. Engl.* **2019,** *58* (29), 10003-10007.
(45) Zayed, M.; Ahmed, A. M.; Shaban, M. Synthesis and characterization of nanoporous ZnO and Pt/ZnO thin films for dye degradation and water splitting applications. Int. J. Hydrogen Energ **2019,** *44* (33), 17630-17648.
(46) Zhang, N.; Han, C.; Xu, Y.-J.; Foley Iv, J. J.; Zhang, D.; Codrington, J.; Gray, S. K.; Sun, Y. Near-field dielectric scattering promotes optical absorption by platinum nanoparticles. *Nat. Photonics* **2016,** *10* (7), 473-482.
(47) Zhang, N.; Han, C.; Fu, X.; Xu, Y.-J. Function-Oriented Engineering of Metal-Based Nanohybrids for Photoredox Catalysis: Exerting Plasmonic Effect and Beyond. *Chem* **2018,** *4* (8), 1832-1861.

(48) Zhang, D.; Peng, L.; Liu, K.; Garcia, H.; Sun, C.; Dong, L. Cobalt nanoparticle with tunable size supported on nitrogen-deficient graphitic carbon nitride for efficient visible light driven H_2 evolution reaction. *Chem. Eng. J.* **2020,** *381*, 122576.
(49) Ye, L.; Wang, D.; Chen, S. Fabrication and Enhanced Photoelectrochemical Performance of MoS_2/S-Doped g-C_3N_4 Heterojunction Film. *ACS Appl. Mater. Interfaces* **2016,** *8* (8), 5280-9.
(50) Yu, X.; Huang, J.; Zhao, J.; Liu, S.; Xiang, D.; Tang, Y.; Li, J.; Guo, Q.; Ma, X.; Zhao, J. Efficient visible light photocatalytic antibiotic elimination performance induced by nanostructured Ag/AgCl@Ti^{3+}-TiO_2 mesocrystals. *Chem. Eng. J.* **2021,** *403*, 126359.
(51) Ran, J.; Gao, G.; Li, F. T.; Ma, T. Y.; Du, A.; Qiao, S. Z. Ti_3C_2 MXene co-catalyst on metal sulfide photo-absorbers for enhanced visible-light photocatalytic hydrogen production. *Nat Commun* **2017,** *8*, 13907.
(52) Liu, H.; Cheng, S.; Wu, M.; Wu, H.; Zhang, J.; Li, W.; Cao, C. Photoelectrocatalytic Degradation of Sulfosalicylic Acid and Its Electrochemical Impedance Spectroscopy Investigation. *J. Phys. Chem. A.A* **2000,** *104* (30), 7016-7020.
(53) Zheng, X.; Liu, K.; Chen, L.; He, H.; Chen, L.; Sun, C. CoO_x Particles in Polymeric N-Doped Carbon Nanotube Applied for Photocatalytic H_2 or Electrocatalytic O_2 Evolution. *Polymers (Basel)* **2019,** *11* (11).
(54) Shi, X.; Zhang, J.; Cui, G.; Deng, N.; Wang, W.; Wang, Q.; Tang, B. Photocatalytic H_2 evolution improvement for H free-radical stabilization by electrostatic interaction of a Cu-BTC MOF with ZnO/GO. *Nano Res.* **2017,** *11* (2), 979-987.
(55) Bai, X.; Wang, L.; Zong, R.; Zhu, Y. Photocatalytic Activity Enhanced via g-C_3N_4 Nanoplates to Nanorods. *J. Phys. Chem. C.* **2013,** *117* (19), 9952-9961.

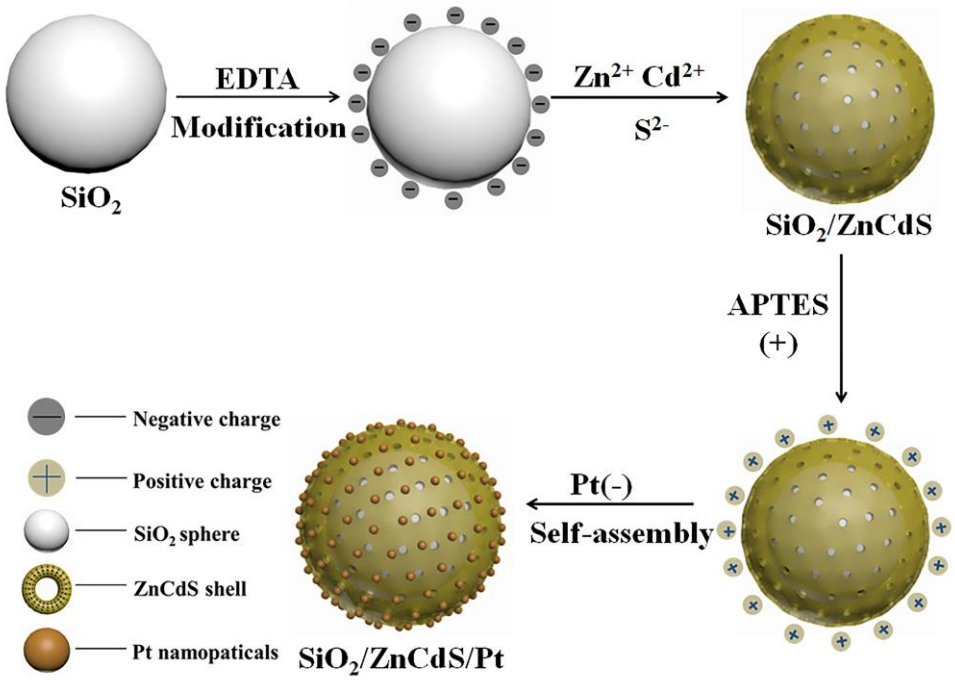

Scheme 1 Schematic illustration of the synthesis process of SiO_2/ZnCdS/Pt photocatalyst.

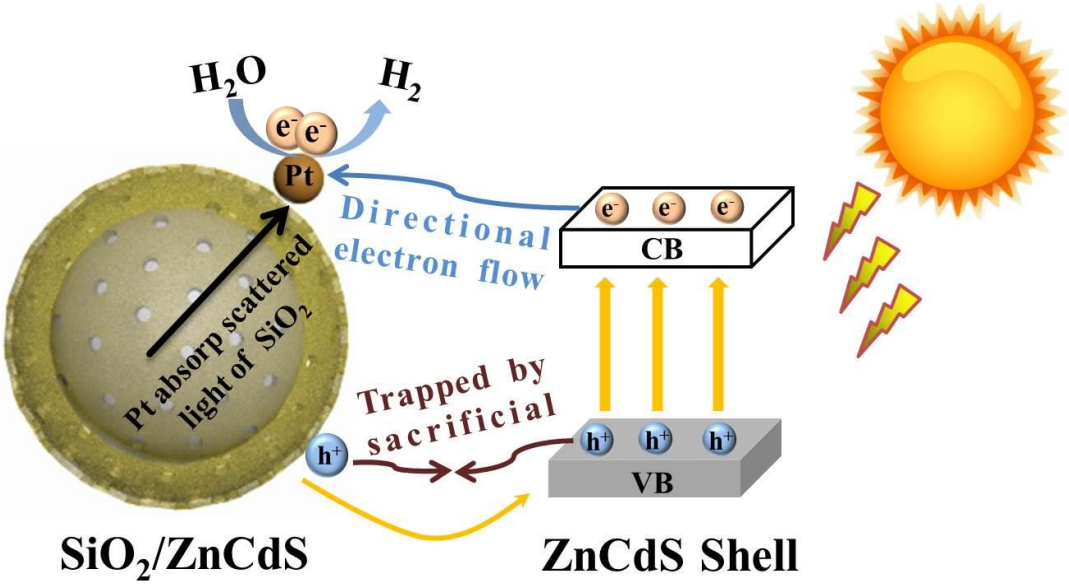

Scheme 2 Schematic illustration of the mechanism for hydrogen production over SiO_2/ZnCdS/Pt.

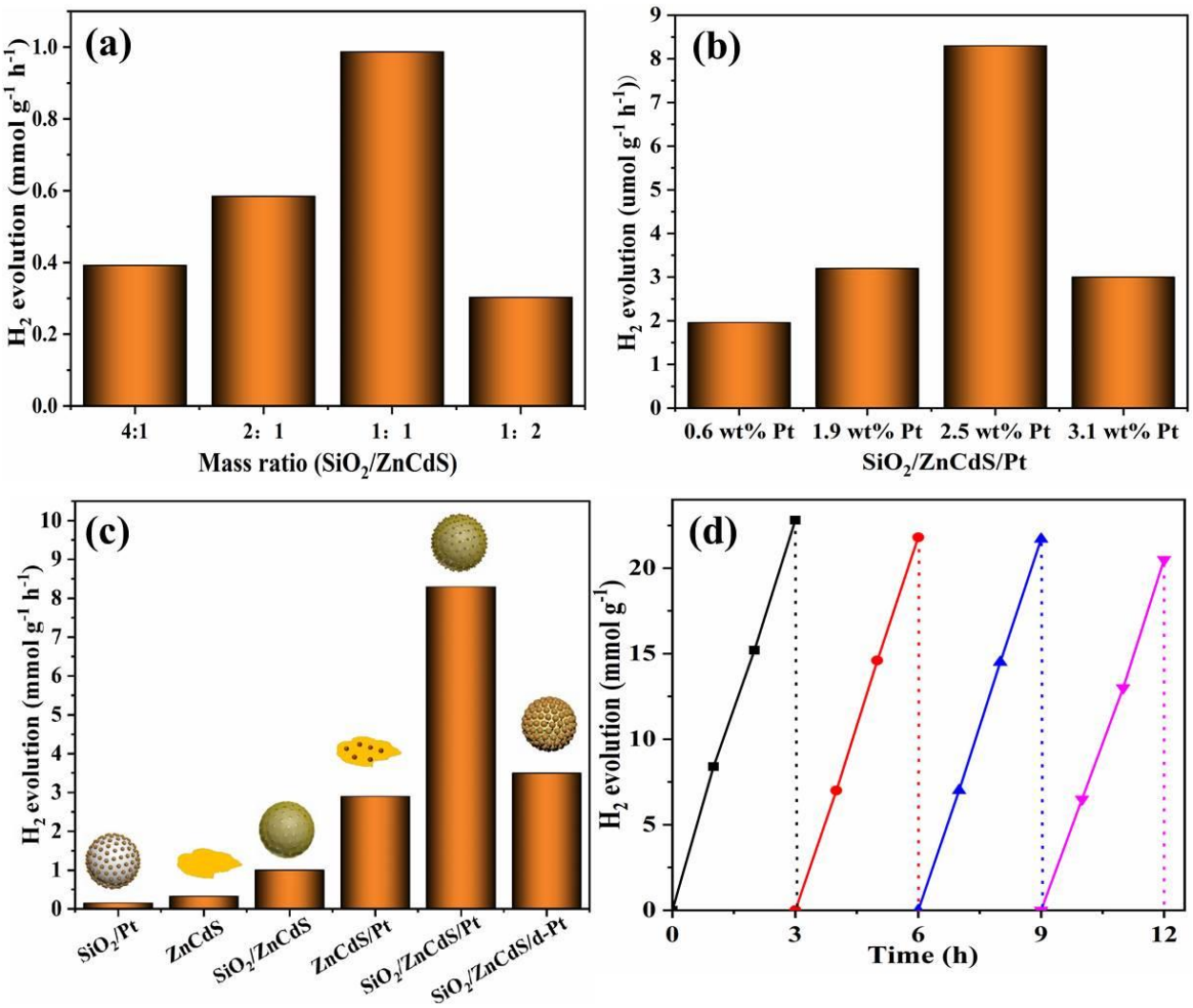

Figure 1 (a) The photocatalytic H_2-production activity of SiO_2/ZnCdS with different mass ratios of SiO_2 and ZnCdS. (b) The photocatalytic H_2-production activity of SiO_2/ZnCdS/Pt with different Pt loadings. (c) The photocatalytic H_2-production activity of different samples. (d) Photocatalytic H_2-production of SiO_2/ZnCdS/Pt photocatalyst upon four consecutive reuses.

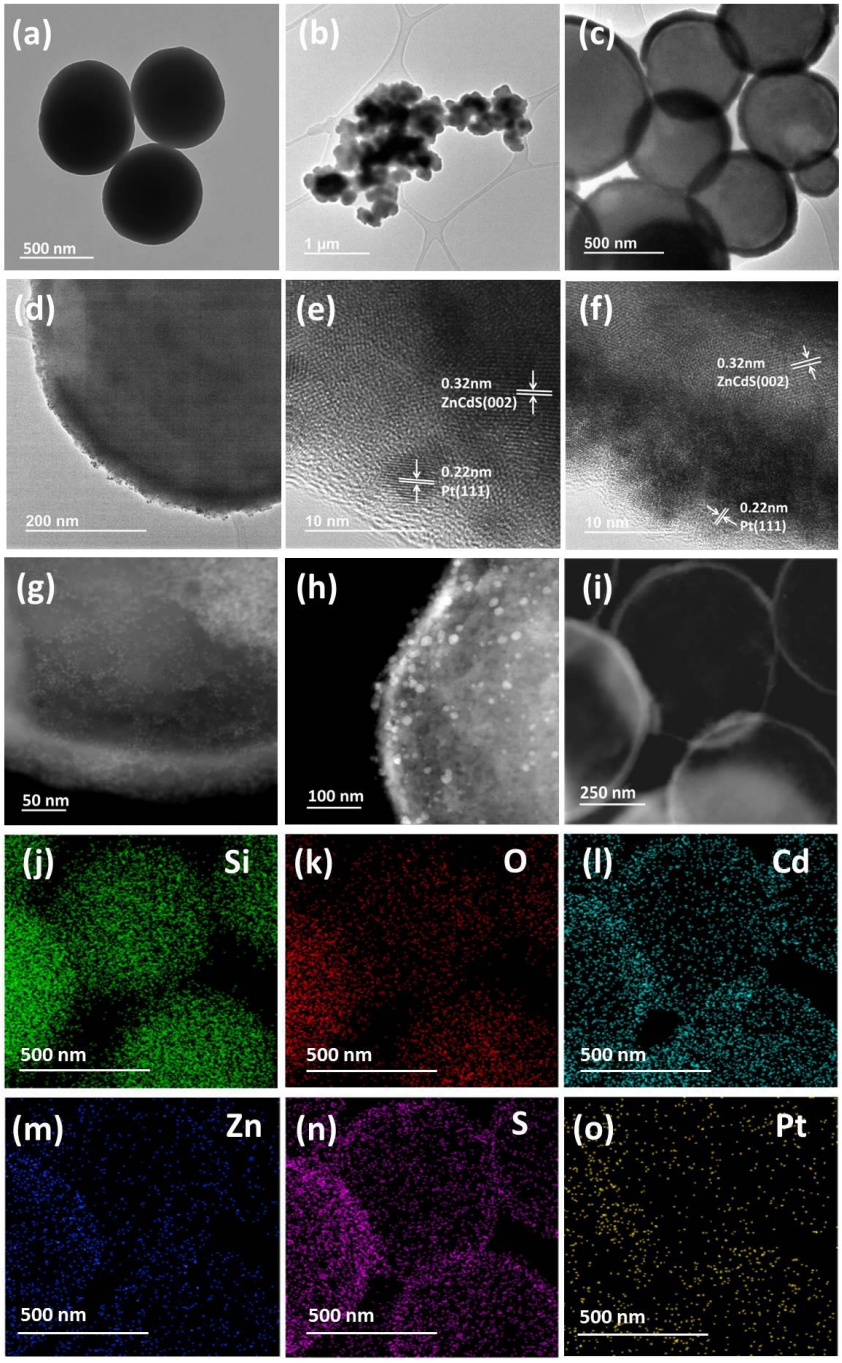

Figure 2 TEM images of (a) SiO_2, (b) ZnCdS, (c) SiO_2/ZnCdS, (d-e) SiO_2/ZnCdS/Pt, (f) HRTEM image of SiO_2/ZnCdS/d-Pt, dark-field transmission electron microscopy (DF-TEM) images of (g) SiO_2/ZnCdS/Pt prepared by the self-assembly method, (h) SiO_2/ZnCdS/d-Pt prepared by the photo-deposition method, (i-o) Energy dispersive spectrometer (EDS) mappings of SiO_2/ZnCdS/Pt.

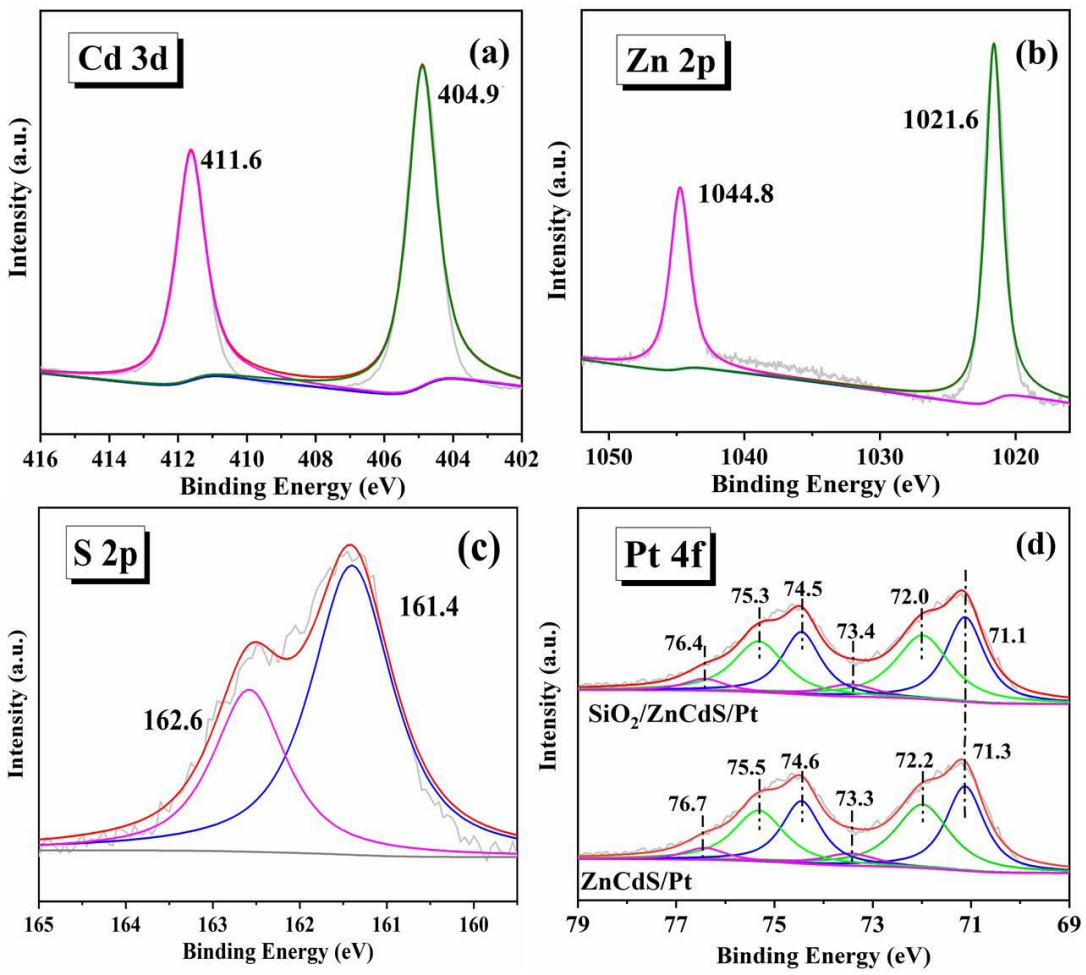

Figure 3 High-resolution XPS spectra of (a) Cd 3d, (b) Zn 2p, (c) S 2p of SiO_2/ZnCdS/Pt and (d) Pt 4f of SiO_2/ZnCdS/Pt and ZnCdS/Pt.

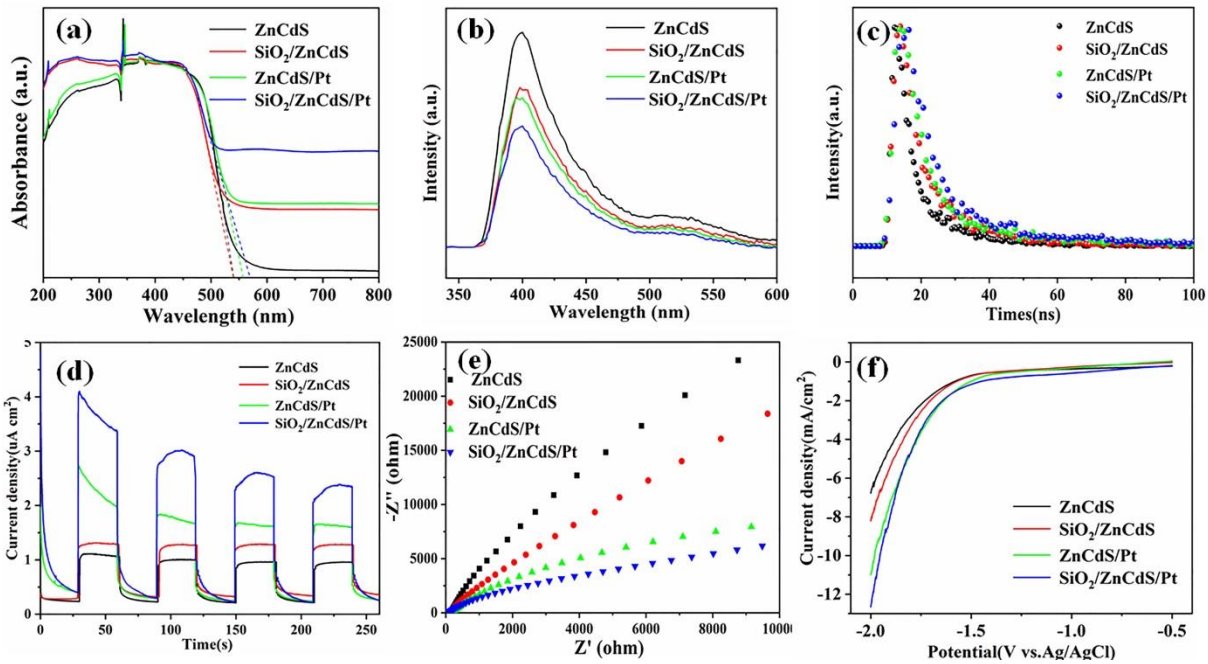

Figure 4 (a) UV-vis diffuse reflectance spectra, (b) Photoluminescence spectra, (c) Time-resolved fluorescence spectra, (d) Transient photocurrent responses under visible light irradiation, (e) Electrochemical impedance spectra and (f) Polarization curves of catalysts.

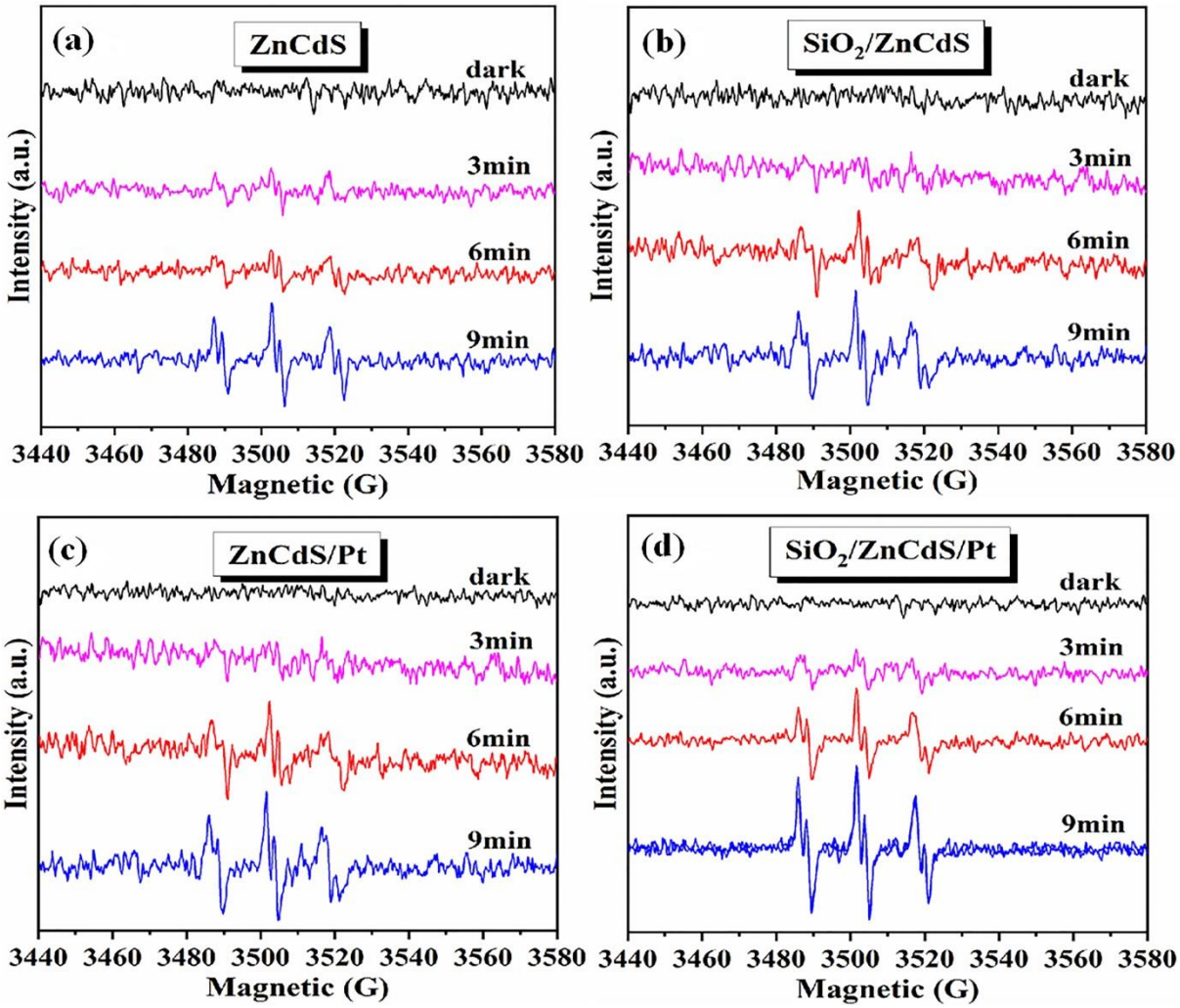

Figure 5 EPR spectra of H• trapping by POBN (POBN-H•) for (a) ZnCdS, (b) SiO_2/ZnCdS (c) ZnCdS/Pt and (d) SiO_2/ZnCdS/Pt samples.

Table 1 Parameters obtained from time-resolved PL decay curves.

Samples	τ_1 (ns) (Rel.%)	τ_2 (ns) (Rel.%)	τ_v (ns)	K_{ENT}	Φ_{ENT}
ZnCdS	4.01 (57.8%)	16.5 (42.2%)	13.3	0.188	0.753
SiO_2/ZnCdS	4.22 (50.5%)	24.9 (49.5%)	21.8	0.196	0.827
ZnCdS/Pt	4.35 (42.5%)	34.9 (57.5%)	32.3	0.201	0.874
SiO_2/ZnCdS/Pt	4.40 (38.8%)	42.2 (61.2%)	39.5	0.203	0.893

TOC

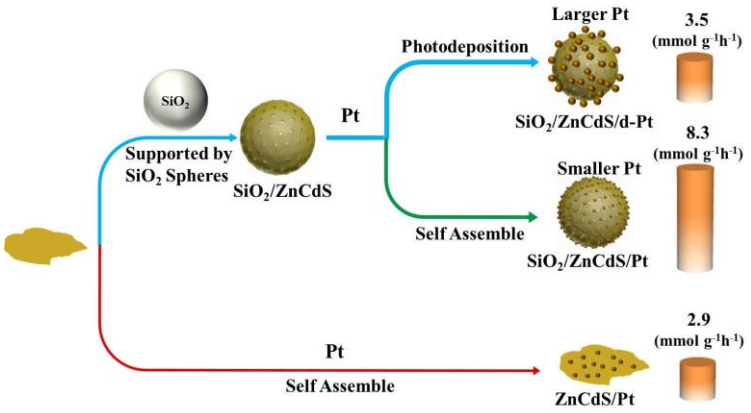

In this paper, an artistic structure of SiO_2/ZnCdS/Pt was constructed. A synergistic effect between SiO_2 sphere and Pt nanoparticles enhances the photocatalytic performance of the system. Meanwhile, catalyst SiO_2/ZnCdS/d-Pt prepared by traditional photo-depositing Pt on SiO_2/ZnCdS are less active than the catalyst SiO_2/ZnCdS/Pt prepared by self-assemble method. The Pt nanoparticles in SiO_2/ZnCdS/Pt sample are much smaller than those in SiO_2/ZnCdS/d-Pt sample, which suggests the size-dependent effect of the Pt nanoparticles on the photocatalytic performance.